Journal of Neuroinflammation

RESEARCH

Open Access

Chemerin-9 is neuroprotective in APP/PS1 transgenic mice by inhibiting NLRP3 inflammasome and promoting microglial clearance of Aβ

Jiawei Zhang[1,2,3†], Yaxuan Zhang[1,3†], Lan Liu[1,3], Mengyuan Zhang[2], Xiaojie Zhang[1,3], Jiangshan Deng[1,3], Fei Zhao[1,3], Qing Lin[2], Xue Zheng[4], Bing Fu[4], Yuwu Zhao[1,3*] and Xiuzhe Wang[1,3*]

Abstract

Background Alzheimer's disease (AD) is a prevalent neurodegenerative disorder worldwide, and microglia are thought to play a central role in neuroinflammatory events occurring in AD. Chemerin, an adipokine, has been implicated in inflammatory diseases and central nervous system disorders, yet its precise function on microglial response in AD remains unknown.

Methods The APP/PS1 mice were treated with different dosages of chemerin-9 (30 and 60 μg/kg), a bioactive nonapeptide derived from chemerin, every other day for 8 weeks consecutively. The primary mouse microglia were stimulated by amyloid beta 42 ($A\beta_{42}$) oligomers followed by treatment with chemerin-9 in vitro. ChemR23 inhibitor α-NETA was further used to investigate whether the effects of chemerin-9 were ChemR23-dependent.

Results We found that the expression of chemerin and ChemR23 was increased in AD. Intriguingly, treatment with chemerin-9 significantly ameliorated Aβ deposition and cognitive impairment of the APP/PS1 mice, with decreased microglial proinflammatory activity and increased phagocytic activity. Similarly, chemerin-9-treated primary microglia showed increased phagocytic ability and decreased NLRP3 inflammasome activation. However, the ChemR23 inhibitor α-NETA abolished the neuroprotective microglial response of chemerin-9.

Conclusions Collectively, our data demonstrate that chemerin-9 ameliorates cognitive deficits in APP/PS1 transgenic mice by boosting a neuroprotective microglial phenotype.

Keywords Alzheimer's disease, Microglia, Chemerin, ChemR23, NLRP3 inflammasome, Phagocytosis

†Jiawei Zhang and Yaxuan Zhang have contributed equally to this work.

*Correspondence:
Yuwu Zhao
zhaoyuwu2005@126.com
Xiuzhe Wang
xiuzhewang@hotmail.com
Full list of author information is available at the end of the article

Graphical Abstract

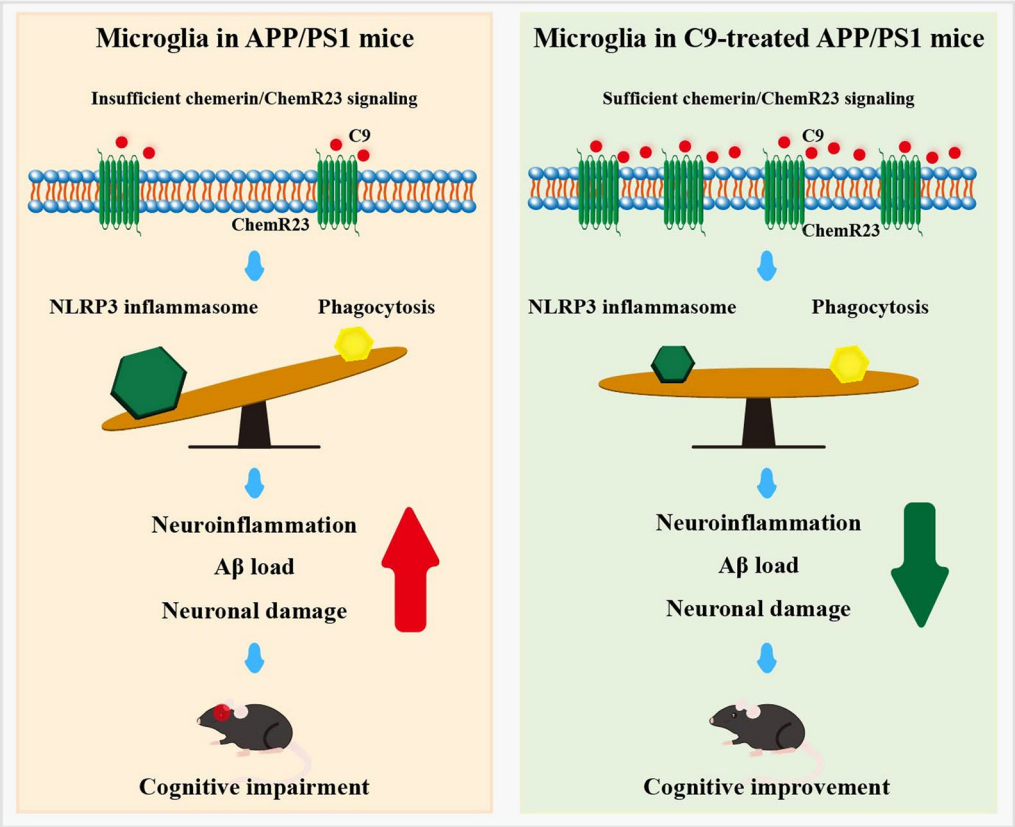

Introduction

Alzheimer's disease (AD) is a progressive neurodegenerative disorder characterized by cognitive deficits, as well as changes in personality and behavior [1]. There are currently multiple hypotheses being proposed to elucidate AD pathogenesis, with the amyloid-β (Aβ) hypothesis being widely recognized as one of the most strongly evidenced. The available data from both preclinical and clinical studies have established a close association between the imbalance between Aβ generation and clearance and the pathogenesis of AD [2]. Furthermore, Aβ-induced microglia-mediated neuroinflammation is a direct cause of neuronal damage and synapse loss, which significantly contributes to the progression of AD [3, 4].

Microglia are the resident macrophage cells of the central nervous system with immune-modulating and phagocytic capabilities [5, 6]. As with periphery macrophages, microglia exhibit a marked alteration in their functions and phenotypes in response to disruptions in their microenvironment [7]. In the pathogenesis of AD, microglia prompt the conversion of a resting type into an active phenotype which promotes the phagocytosis of Aβ and neuronal debris. However, sustained activation of microglia causes excessive release of inflammatory mediators that transform microglia from a protective phenotype to a detrimental phenotype, eventually leading to neuronal damage. The aforementioned implies that the restoration of microglial phenotype from the pathological state to the healthy state, or alternatively, the specific activation of microglia may be effective therapeutic strategies for AD. For example, Zerumbone treatment facilitated the transition of microglial phenotype from the classic to the alternative phenotype, resulting in a reduction in Aβ deposition and improvement in cognition [8].

Chemerin, a chemoattractant protein encoded by the retinoic acid receptor responder 2 protein (Rarres2) gene, has recently been identified as an adipokine closely related to the pathogenesis of metabolic syndrome and inflammatory diseases [9–11]. Chemerin is biosynthesized as a 163-amino-acid preprochemerin and is secreted as prochemerin once its 20 amino acid N-terminal signal peptide has been truncated. Inactive

prochemerin is then C-terminally cleaved by different proteases, yielding active chemerin peptides that are named based on their last C-terminal amino acid [12]. Chemerin-9 is a nonapeptide derived from chemerin that has the majority of the activity comparable to that of the full-length protein and is sufficient to activate the G protein-coupled receptor ChemR23 (namely Cmklr1) [13]. It has been reported that chemerin-9 improves atherosclerosis in ApoE$^{-/-}$ mice by regulating the inflammatory phenotype of macrophages [14]. Meanwhile, recent evidence has demonstrated that the chemerin/ChemR23 axis is implicated in numerous central nervous system disorders, including stroke and multiple sclerosis [15–18]. Moreover, our recent study has shown that chemerin-9 can ameliorate cognitive dysfunction in diabetic mice by alleviating oxidative stress and inhibiting NLRP3 inflammasome activation [19]. However, the role of chemerin-9 and its functional mechanism in AD remain elusive. Therefore, our present study aimed to uncover the effect and mechanism of chemerin-9 on microglia in AD by using primary microglia as a cell model and APP/PS1 mice as an animal model in vitro and in vivo, respectively.

Materials and methods

Animals and drug treatment

Male APPswe/PS1dE9 and C57BL/6 J littermates were purchased from the Shanghai Nanfang Research Center for Model Organisms (Shanghai, China). The genotypes were confirmed by PCR using tail tissue DNA. The mice were accommodated within a controlled environment that was free of specific pathogens, with an ambient temperature range of 20–25 °C and a light cycle of 12 h on and 12 h off. They had unrestricted access to food and water until they reached 8 months of age. Afterward, the mice were classified into four groups: C57BL/6 J littermate wild-type controls (WT), APPswe/PS1dE9 vehicle-treated controls (APP/PS1), APPswe/PS1dE9 treated with chemerin-9 at a dosage of 30 μg/kg body weight (APP/PS1 + C9-L), and APPswe/PS1dE9 treated with chemerin-9 at a dosage of 60 μg/kg body weight (APP/PS1 + C9-H). Chemerin-9 (C9, Item # 7117, Tocris Bioscience, Bristol, UK), a bioactive derivative of full-length chemerin consisting of C-terminal amino acids 148–156, was dissolved in sterile PBS. The dose selected for this study was based on our previous literature [19]. All groups of mice were treated intraperitoneally every other day for eight weeks consecutively. In accordance with the guidelines established by the National Institutes of Health (NIH) for the Care and Use of Laboratory Animals, all procedures were authorized by the ethical committee on animal welfare of Shanghai Sixth People's Hospital Affiliated to Shanghai Jiao Tong University School of Medicine.

Y maze test

The working memory of mice was evaluated through spontaneous alternations at the Y-maze. The Y maze equipment consists of three equidistant arms placed at a 120-degree angle, measuring 15 cm in height, 30 cm in length, and 8 cm in width. The mice are introduced into the central region of the maze and permitted to navigate the apparatus freely for 5 min. The quantity of arm entries was captured on video and then automatically calculated by EthoVision XT software (Noldus). The concept of correct alternation was established to denote the sequential entry into three distinct arms. On the other hand, the notion of max alternation was introduced to signify the count of possible alternations, which is determined by subtracting 2 from the total number of arms entered. The percentage of alternation was computed by dividing the number of correct alterations by the max alternation.

Morris water maze test

The spatial learning and memory of mice were assessed using the Morris water maze (MWM) test, which was conducted with slight modifications in accordance with our previous methodology [19]. Briefly, the equipment utilized in the experiment comprised a round basin with a height of 50 cm and a diameter of 120 cm that was filled with tepid water at a temperature of 23 ± 2 °C. Additionally, a small circular platform with a diameter of 10 cm was positioned in the center of the objective quadrant, and it was submerged 1.0 cm below the water surface. During the orientation navigation test, conducted four times a day for five consecutive days, mice were granted 60 s to explore the submerged platform. Any mice unable to locate the platform within the allotted time frame were artificially guided to the platform and kept there for 10 s. The escape latency was measured as the time required to reach the platform during each trial. On the sixth day, a probe trial was performed during which mice were allowed to navigate freely for 60 s without the platform, and a video tracking system, EthoVision® XT 15, automatically assessed the number of times the mice crossed the platform, the time spent in the target quadrant, and the average swimming speed.

Nissl staining

Upon completion of behavioral experiments, the mice underwent transcardial perfusion with PBS, followed by 4% paraformaldehyde. The brains were subsequently embedded in paraffin and sliced into 5 μm thick sections for further staining. A deparaffinization process was subsequently performed on the brain sections, after which they were gradually rehydrated through the use of graded concentrations of ethanol. Finally, the brain sections

underwent treatment with a conventional Nissl staining solution, and high-resolution images were obtained via optical microscope imaging.

Golgi staining

Golgi staining was performed to detect the morphology of the dendritic spines in the hippocampus. Following transcardial perfusion with PBS and 4% paraformaldehyde, the brains of mice were immediately taken and immersed in fixative for more than 48 h. The hippocampus was cut into 2–3 mm thick tissue and the tissue was gently rinsed several times with 0.9% NaCl solution and placed in a 45 ml round-bottomed EP tube. The tissue was then transferred to Golgi staining solution, and placed in a cool and ventilated place for 14 days. After finishing impregnation, the tissue was washed thrice with distilled water and immersed in 80% glacial acetic acid overnight. After the tissue became soft, it was washed with distilled water and immersed in 30% sucrose. Then the specimens were sectioned coronally at 100 μm by using a vibratome, mounted onto gelatin-coated slides, and kept in black wet boxes at 4 °C overnight. The slices were soaked with ammonia for 15 min, followed by washing with distilled water for 1 min. After soaking in Kodak Film Fix for 15 min, the slices were rinsed with distilled water for 3 min, and sealed with glycerol gelatin. The images were captured using a Nikon Eclipse E100 microscope. Dendritic spines were counted and statistically analyzed using ImageJ software. The spine density was measured and expressed as the number of spines per 10 μm dendrite.

Thioflavin-S

Thioflavin-S staining was performed as previously described [20]. Briefly, the brain sections underwent deparaffinization followed by hydration through a graded ethanol series. Subsequently, the sections were subjected to 1% Thioflavin S staining solution for 5 min and then differentiated in 70% ethanol for 1 min before being mounted. An Olympus microscope was used to capture images of all the sections.

RNA scope for in situ hybridization (ISH) combined with immunofluorescence staining

The brains of mice were promptly removed following transcardial perfusion with PBS, fixed in 4% paraformaldehyde, paraffin-embedded, and sliced into 5 μm thick sections. The RNAscope Fluorescent Multiplex Assay was utilized for in situ hybridization, wherein the sections underwent processing with the RNAscope® Fluorescent Multiplex Reagent Kit (Advanced Cell Diagnostics, Newark, CA) in accordance with the guidelines provided by the manufacturer. After being subjected to 4% paraformaldehyde fixation for 30 min at 4 °C, the sections were dehydrated in graded ethanol and subsequently treated with protease for 30 min at room temperature. Following this, the ChemR23 mRNA probe (Advanced Cell Diagnostics, Newark, CA) was employed for the hybridization process in the ACD HybEZ™ II oven at 40 °C for 2 h. The sections were then subjected to a sequential incubation process in the ACD HybEZ™ II oven, maintained at a temperature of 40 °C, utilizing amplification reagents. The amplification process was carried out in three stages, namely AMP-1 for 30 min, AMP-2 for 15 min, and AMP-3 for 30 min. Similarly, the process of immunofluorescence staining was carried out using identical steps to those employed in the immunofluorescence assay. Finally, the sections were observed under a fluorescence microscope.

RNA sequencing

To conduct RNA Sequencing (RNAseq) experiments, four hippocampus samples from each group were selected at random. Total RNAs were extracted by employing the Trizol reagent kit (Invitrogen, CA, USA) in accordance with the manufacturer's guidelines. The quality of RNA was assessed using the Agilent 2100 Bioanalyzer and confirmed through RNase-free agarose gel electrophoresis. Subsequently, the mRNAs that had been enriched were fragmented into shorter fragments with the aid of a fragmentation buffer. These fragments were then transcribed into cDNA in a reverse manner, utilizing the NEBNext Ultra RNA Library Prep Kit for Illumina (NEB #7530, New England Biolabs, MA, USA). The cDNA library that was generated was sequenced by Gene Denovo Biotechnology Co. (Guangzhou, China) using Illumina Novaseq6000 technology. The reads obtained through sequencing machines underwent further filtration using fastp (version 0.18.0) to obtain high-quality clean reads. The differential expression analysis of RNA was conducted between two different groups through the use of DESeq2 software. Differentially expressed genes (DEGs) were identified by considering those with a false discovery rate (FDR) parameter below 0.05 and an absolute fold change of 2 or greater. A functional analysis was conducted on the DEGs of each group, which entailed enrichment of Kyoto Encyclopedia of Genes and Genomes (KEGG) pathways and gene set enrichment analysis (GSEA).

Preparation of Aβ oligomers

To prepare Aβ oligomers, 1 mg of $A\beta_{42}$ peptide (#010080051, HarO Life, Shanghai, China) was dissolved in 221.7 μl of cold HFIP (1,1,1,3,3,3-hexafluoro-2-propanol) to create a 1mM concentration solution. The solution was left at room temperature for an hour

and then cooled on ice for 10 min. The resulting solution was divided into non-siliconized microcentrifuge tubes, with each containing 0.45 mg of $A\beta_{42}$ in 100 µl solution, before being dried overnight at room temperature. The dried residues were then dissolved in 20 µl of dimethyl sulfoxide (DMSO) and mixed with F12 medium to create a 100 µM stock solution. The solution was left to incubate at 4 °C overnight, resulting in the formation of Aβ oligomers, which were further checked by western blot employing 6E10 antibody (Suppl. Figure 1).

Isolation and treatment of primary microglia

As was previously reported, primary microglial cells were collected from the pups on post-natal day 1 [21, 22]. Briefly, hippocampi and cortices from 1-day-old C57BL/6 J mice were isolated with the aid of a microscope and placed into ice-cold HBSS. After the meninges and leptomeningeal blood vessels were removed, the brain tissues were triturated and digested with 0.125% trypsin at 37 °C for 20 min. After neutralization and centrifugation at 1000 rpm for 5 min, the cells were plated in T75 flasks and cultivated in glial media consisting of DMEM supplemented with 10% fetal bovine serum and 100 µg/ml penicillin/streptomycin at 37 °C, 5% CO2 in order to generate mixed glial cultures. Every 4–5 days, half of the medium was changed and a confluent glial monolayer was established within 10–14 days. To harvest microglia, the flasks were placed in a 37 °C shaker for 15 min at 200 rpm. The media containing microglia was collected in a new tube and centrifuged at 1000 rpm for 5 min. After shaking, trypsin diluted 1:3 was added to the T75 flasks and incubated at 37 °C for 30 min with occasional shaking until the astrocyte layer was detached. Subsequently, the astrocyte layer was carefully removed and discarded. Microglia culture medium was then added to the flask, and the flask was shaken for 15 min to further obtain microglia beneath the astrocyte layer. Obtained microglia seeded in PDL-coated plates for the following experiment. Cell cultures were enriched for microglia by washing with DMEM for a minute, and then incubating a 1:3 dilution of trypsin in warm DMEM at 37 °C with 5% CO2 for 30 min with occasional shaking. The primary microglia were pretreated with or without the ChemR23 inhibitor α-NETA (10 µM) (31059-54-8, GlpBio, California, USA) for 2 h, followed by co-incubation with Aβ (5 µM) and chemerin-9 (500 nM) for 24 h.

For conditioned medium preparation, microglial cells were plated on 6-multiwell in microglial medium (DMEM + 10% FBS) at a density of 1×10^6 cells/well. The next day, microglial media was replaced with neuronal culture medium (neurobasal medium + GlutaMAX + B-27). After 24 h, conditioned medium (CM) was collected and centrifuged 1000 rpm for 5 min, then used for subsequent experiments or stored at − 80 °C.

Isolation and treatment of primary neuron

Primary hippocampal neurons were prepared from hippocampi and cortices of embryos at embryonic day 17 (E17). Briefly, brains were harvested and immersed in ice-cold HBSS, and the hippocampi and cortices were dissected after removing the meningeal and leptomeningeal vessels. Then, the hippocampi and cortices were minced and digested with 2 mg/ml papain (Macklin, Shanghai, China) and 0.1 mg/ml DNase (Macklin, Shanghai, China) at 37 °C for 30 min. After terminating digestion with FBS, the tissue was triturated gently with a 1 ml pipette to obtain a single-cell suspension which was plated onto glass coverslips coated with poly-L-lysine at the density of 95 cells/mm^2. After 3 h, the medium was replaced with neuronal culture medium containing neurobasal medium, GlutaMAX and B-27 (all from Gibco, California, USA). One-half of the culture medium was changed every 2–3 days and all experiments were performed at 5 days in vitro. The primary neurons were incubated for 24 h with CM harvested from differently treated primary microglia.

Aβ1—42 uptake assay

HiLyte Fluor™ 488-labeled Aβ1–42 peptide was prepared according to the instruction of the manufacturer (Anaspec, Fremont, USA). Briefly, the lyophilized Aβ42 peptide powder was dissolved in 1.0% NH4OH and immediately diluted with PBS to a concentration of 1 mg/ml. If not used immediately, the reconstituted peptide was stored at − 80 °C.

Primary microglial cells were plated on coverslips in a 24-well plate for 24 h. Then, the cells were pretreated with or without the ChemR23 inhibitor α-NETA (10 µM) for 2 h, followed by co-incubation with HiLyte Fluor™ 488-labeled Aβ1–42 (5 µM) and chemerin-9 (500 nM) for 24 h. After fixation with 4% PFA for 20 min and permeabilization with 0.1% Triton X-100 for 30 min at room temperature, cells were washed with PBS three times and blocked with 5% donkey serum for 1 h. Next, cells were incubated with primary anti-Iba1 antibody (1:250) at 4 °C overnight and then washed three times with PBST. Alexa 555-conjugated donkey anti-rabbit secondary antibody at a 1:1000 dilution was then applied for 1 h at room temperature. Nuclei were stained with DAPI for 5 min at room temperature. The cells were finally analysed using a confocal microscope (A1, NIKON, Tokyo, Japan).

qRT-PCR

The qRT-PCR was conducted in accordance with our previous description [19]. The RNAeasy™ animal RNA

isolation kit with a spin column was employed to extract total RNAs from the hippocampus and primary microglia, following the manufacturer's protocol. Utilizing the PrimeScript™ RT Master Mix (Perfect Real Time), isolated RNAs were subjected to reverse transcription to generate cDNA. The qPCR assay was carried out on the Applied Biosystems 7500 Real-Time PCR System (Applied Biosystems, CA, USA), employing TB Green™ Premix Ex Taq™ II (Tli RNaseH Plus). The amplification parameters utilized in this study involved an initial step of 95℃ for 30 s, followed by 40 cycles of 95℃ for 5 s and 60℃ for 34 s, 95℃ for 15 s, 60℃ for 60 s, and 95℃ for 15 s. The $2^{-\Delta\Delta Ct}$ method was employed to determine the gene expression levels. The relative mRNA expression level in the WT or control group (target mRNA/β-actin value) was taken as the baseline of 100%, and the mRNA values in the APP/PS1 or Aβ-treated group were converted into fold changes after being compared with the WT or control group.

To detect transcriptions, the following PCR primer sequences were employed: β-actin, F: 5′-GTGACGTTG ACATCCGTAAAGA-3′, R: 5′-GTAACAGTCCGCCTA GAAGCAC-3′; ChemR23, F: 5′-TACGACGCTTAC AACGACTCC-3′, R: 5′-TAGGAGACCGAGGAAGCA CA-3′; chemerin, F: 5′-GAGGAGTTCCACAAACAC CCA-3′, R: 5′- CTTCTCCCGTTTGGTTTGATTG-3′.

Western blot analysis

The protein in the hippocampus and cultured primary microglia were analyzed via Western blotting, following the methodology we had previously described [19], albeit with minor modifications. To obtain a homogenized solution of the hippocampi and cultured primary microglia, RIPA buffer was utilized in conjunction with protease and phosphatase inhibitors and subjected to sonication. The concentration of protein was subsequently determined using the BCA kit (Beyotime, Nanjing, China). An equivalent quantity of protein was loaded onto sodium dodecyl sulfate-polyacrylamide gel electrophoresis (SDS-PAGE) for various samples, which were then transferred onto polyvinylidene fluoride (PVDF) membranes. After blocking with 5% BSA in TBS-T, the membranes were subjected to overnight incubation at 4 °C with the primary antibodies listed below: synaptophysin (SYN) (A19122, 1:1000, Abclonal, Wuhan, China), postsynaptic density protein-95 (PSD95) (A6194, 1:1000, Abclonal, Wuhan, China), nucleotide-binding oligomerization domain-like receptor protein 3 (NLRP3) (GB114320, 1:1000, Servicebio, Wuhan, China), apoptosis-associated speck-like protein containing a CARD (ASC) (10500-1-AP, 1:1000, Proteintech, IL, USA), caspase1 (A0964, 1:1000, Abclonal, Wuhan, China), APP (GB112075, 1:1000, Servicebio, Wuhan, China), Presenilin 1(PS1) (GB11779, 1:1000, Servicebio, Wuhan, China), PEN2 (A8678, 1:1000, Abclonal, Wuhan, China), BACE1 (A11533, 1:1000, Abclonal, Wuhan, China), Nicastrin (A0128, 1:1000, Abclonal, Wuhan, China), 6E10 (803001, 1:200, Biolegend, San Diego, USA), and β-actin (20536-1-AP, 1:1000, Proteintech, IL, USA). Following three washes with TBS-T, the membranes were treated with a secondary anti-rabbit antibody, namely horseradish peroxidase (HRP)-conjugated immunoglobulin G (IgG) (GB23303, 1:1000, Servicebio, Wuhan, China). The immunoblots were subsequently visualized using the enhanced chemiluminescence (ECL) kit (Invitrogen, CA, USA), with the grayscale value of signals being determined through quantification using ImageJ software.

Immunofluorescence staining

In vivo: The brains of mice were promptly removed following transcardial perfusion with PBS, fixed in 4% paraformaldehyde, paraffin-embedded, and sliced into 5 μm thick sections. A deparaffinization process was then performed on the brain sections, after which they were gradually hydrated through the use of graded concentrations of ethanol. Afterward, the brain sections were subjected to microwave heating to facilitate antigen retrieval. In vitro: The primary microglia were seeded onto glass coverslips in 6-well tissue culture dishes for 24 h, and primary microglia were pretreated with or without the ChemR23 inhibitor α-NETA (10 μM) for 2 h, followed by co-incubation with Aβ (5 μM) and chemerin-9 (500 nM) for 24 h. Afterward, the cells on glass coverslips were washed and fixed with cold 4% paraformaldehyde.

Subsequently, the brain sections or formaldehyde-fixed cells were treated with 5% BSA to block non-specific binding, followed by overnight incubation with nucleotide-binding oligomerization domain-like receptor protein 3 (NLRP3) (GB114320, 1:1000, Servicebio, Wuhan, China), 6E10 (803001, 1:200, Biolegend, San Diego, USA), Clec7a (mabg-mdect, 1:100, InvivoGen, France), and Iba-1 (GB113502, 1:300, Servicebio, Wuhan, China) primary antibodies at 4 °C. The sections and the cells on glass coverslips were then washed thrice with PBS before being incubated with horseradish peroxidase (HRP)-conjugated immunoglobulin G (IgG) secondary antibody for 2 h at room temperature. After the final washes in PBS, DAPI was used to counterstain the nuclei. The sections were examined and analyzed using a fluorescence microscope (three slides per mouse for a corresponding region of interest).

Enzyme-linked immunosorbent assay

In accordance with the manufacturer's instructions, enzyme-linked immunosorbent assay (ELISA) kits were utilized to quantify the levels of interleukin (IL)−1β, IL-6,

TNF-α, $A\beta_{1-40}$, and $A\beta_{1-42}$ in the cortex and hippocampus and cultured primary microglia. In vivo: The brain samples were thawed on ice and homogenized in PBS using an electric tissue grinder. The tissue homogenates underwent centrifugation at 3000× g for 10 min at 4 °C, and the resulting homogenate supernatant was collected and the total protein concentration was determined by BCA Protein Assay Kit. Levels of IL-1β (#EK201B/3, Multisciences, Hangzhou, China), IL-6 (#EK206/3, Multisciences, Hangzhou, China), $A\beta_{1-40}$, (#BPE11681, Langdun, Shanghai, China) and $A\beta_{1-42}$ (#BPE11405, Langdun, Shanghai, China) were evaluated via commercial ELISA kits according to the manufacturer's protocol. In vitro: The primary microglia were initially seeded in 6-well plates and incubated at 37 °C for 24 h. The cells were then subjected to pretreatment with the ChemR23 inhibitor α-NETA (10 μM) for 2 h before being co-incubated with Aβ (5 μM) and chemerin-9 (500 nM) for 24 h. Following collection, the culture medium was centrifuged at 12,000 rpm for 10 min, and then quantified the levels of IL-6 (#EK206/3, Multisciences, Hangzhou, China) and TNF-α (#EK282/4, Multisciences, Hangzhou, China) using mouse ELISA kits.

Calcein-AM and propidium iodide (PI) assays

Cells were stained with live-dead staining kits according to the manufacturer's protocol (Yeasen Biotech, Shanghai, China). After the required treatment, the cells were incubated with the mixture of dyes (2 μl/ml Calcein-AM and 3 μl/ml PI) for 15 min at 37 °C. The results were analysed under a fluorescence microscope (IX53, Olympus, Tokyo, Japan). The red or green signals indicated the dead cells or viable cells, respectively.

Statistical analysis

GraphPad Prism 9 (GraphPad Software Inc., CA, USA) was utilized for statistical analysis. The data were expressed as mean ± standard error of the mean (SEM) and subjected to one-way analysis of variance (ANOVA) with Tukey's post hoc test. For experiments with only two groups, the t-test was employed. In the case of the Morris water maze test's hidden-platform training, the escape latency was analyzed by two-way repeated-measures ANOVA followed by Tukey's post hoc test. Limma package was used to analyze the downloaded human transcriptomic datasets. The level of statistical significance was set at $P < 0.05$.

Results

Increased expression of chemerin and ChemR23 in AD

Firstly, we used the human transcriptomic dataset to analyze chemerin/ChemR23 changes in AD patients. In the dataset of GSE48350 and GSE5281, we found that chemerin mRNA levels were significantly increased in the hippocampus and middle temporal gyrus of patients with AD compared to the nondemented controls (Fig. 1A and Suppl. Tables 1–2). Similarly, we found that ChemR23 mRNA levels were significantly increased in the hippocampus and temporal cortex of patients with AD compared to the nondemented controls in the dataset of GSE5281 and GSE122063 (Fig. 1B and Suppl. Tables 3–4). Then, these alternations of chemerin and ChemR23 were successfully validated in the brain of 10-month-old APP/PS1 transgenic mice, which is a widely used mouse model for AD that harbors familial AD gene mutations. As shown in Fig. 1C and D, APP/PS1 mice exhibited higher levels of chemerin and ChemR23 in the hippocampus and cortex as compared with WT mice. Considering that ChemR23 might be a functional receptor for microglia, we proceeded to analyze the dataset of mice using the CSF1R antagonist PLX5622, which eliminates > 95% of microglia in the brain [23]. The results indicated that the absence of microglia led to a reduction in ChemR23 mRNA levels in the hippocampus and cortex of both WT and AD mice (Fig. 1E), highlighting the specific association between microglia and ChemR23 expression in the brain. In addition, incubation of primary murine microglia with $A\beta_{42}$ oligomers resulted in a significant increase in the transcriptional levels of chemerin and ChemR23 (Fig. 1F). Moreover, we further investigated the co-localization of ChemR23 and microglia using an ISH-immunofluorescence approach which facilitated the detection of ChemR23 signal within microglia. As shown in Fig. 1G and H, a higher level of co-localization of ChemR23 and Iba1 was observed in the hippocampus and cortex of APP/PS1 mice compared with WT mice. These results

(See figure on next page.)

Fig. 1 Abnormally high expression of Chemerin and ChemR23 in AD. **A** Transcriptional up-regulation of Rarres2 in the hippocampus of the GSE48350 database (control, $n = 42$; AD patients, $n = 19$) and in the middle temporal gyrus of the GSE5281 database (control, $n = 12$; AD patients, $n = 16$). **B** Transcriptional up-regulation of Cmklr1 in the hippocampus of the GSE5281 database (control, $n = 12$; AD patients, $n = 10$) and in the temporal cortex of the GSE122063 database (control, $n = 22$; AD patients, $n = 28$). **C**, **D** Transcriptional up-regulation of Rarres2 and Cmklr1 in the hippocampus and cortex of 10-month-old APP/PS1 mice ($n = 4$). (**E**) Transcriptional expression of Cmklr1 in WT and AD mice following CSF1R antagonist PLX5622 (Plx) treatment ($n = 4$). **F** Transcriptional up-regulation of Rarres2 and Cmklr1 in murine primary microglia cultures incubated with Aβ oligomers ($n = 3$). **G**, **H** RNA in situ hybridization of ChemR23 expression and its colocalization with Iba1 (immunostaining)-positive cells in the hippocampus and cortex of 10-month-old WT and APP/PS1 mice. *$P < 0.05$; **$P < 0.01$; ***$P < 0.001$

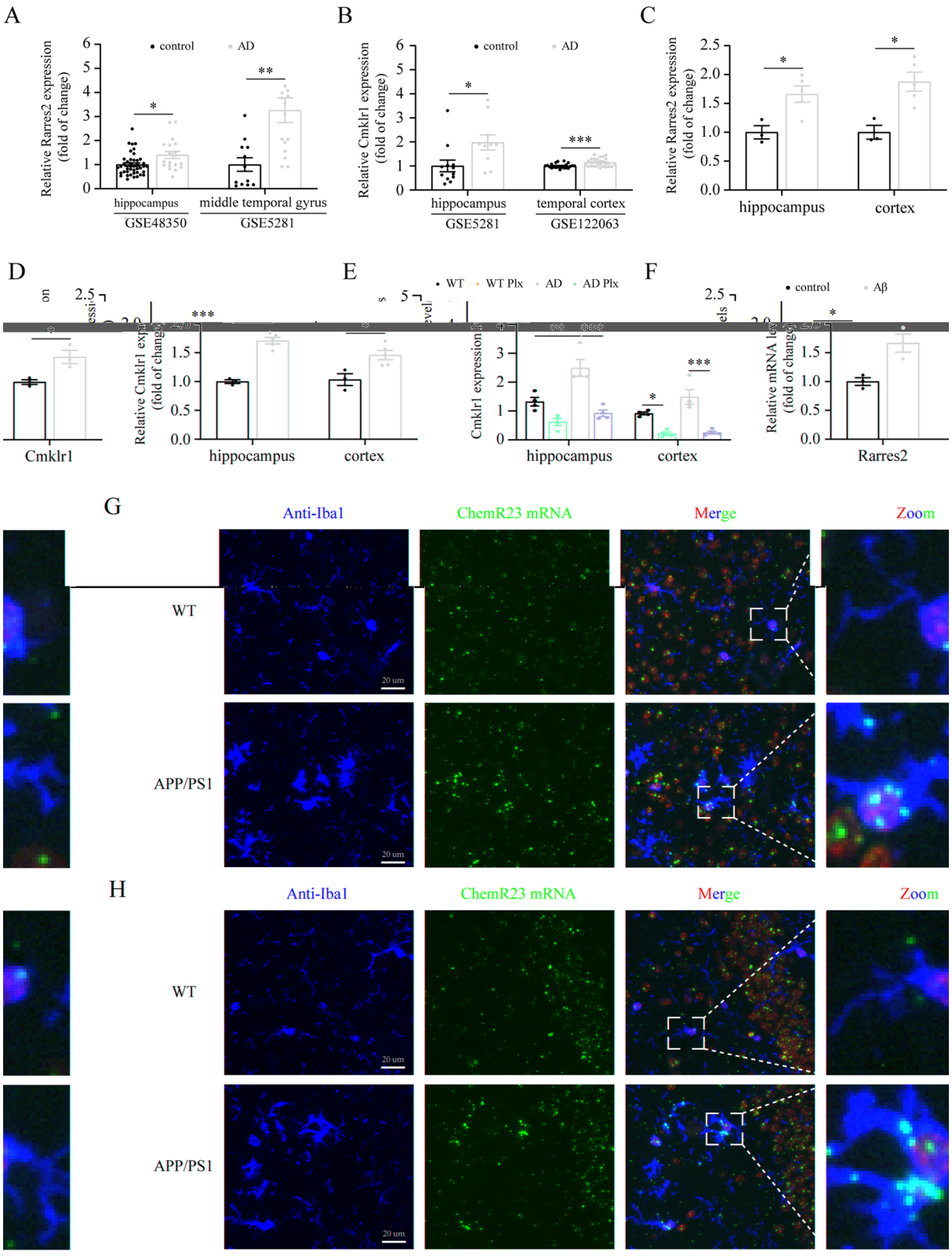

Fig. 1 (See legend on previous page.)

collectively suggest that the brain affected by AD exhibits an upsurge in chemerin/ChemR23 levels, underscoring the potential significance of the chemerin/ChemR23 axis in the pathophysiology of AD.

Chemerin-9 ameliorates cognitive deficits in APP/PS1 mice

We then used the Y-maze and Morris water maze tests to assess the potential effects of chemerin-9, a bioactive derivative of full-length chemerin, on cognitive deficits in APP/PS1 mice (Fig. 2A). As shown in Fig. 2B, the APP/PS1 mice exhibited a significantly lower spontaneous alternation rate in comparison to the WT mice. In contrast, the chemerin-9-L and chemerin-9-H mice demonstrated a marked increase in their spontaneous alternation rate when compared to the APP/PS1 mice, indicating that chemerin-9 treatment effectively improved working memory in AD mice. During the 5-day acquisition period, the MWM test demonstrated a progressive decline in escape latency in all groups tested (Fig. 2C). Nevertheless, the APP/PS1 mice exhibited a significantly higher escape latency on days 4 and 5 than the WT mice. In contrast, the chemerin-9-L mice experienced a significant reduction in escape latency on day 4 compared to the APP/PS1 mice. Additionally, the chemerin-9-H mice showed a significant decrease in escape latency on days 4 and 5 relative to the APP/PS1 mice (Fig. 2C and E). During the probe trial, it was observed that the number of times APP/PS1 mice crossed the platform was significantly lower than that of the WT mice. However, chemerin-9-H mice showed a significant increase in the number of times they crossed the platform compared to APP/PS1 mice. The chemerin-9-L mice did not exhibit an increase in the number of times they crossed the platform compared to APP/PS1 mice (Fig. 2D). Among the groups, there were no obvious differences in swimming speed (Fig. 2F).

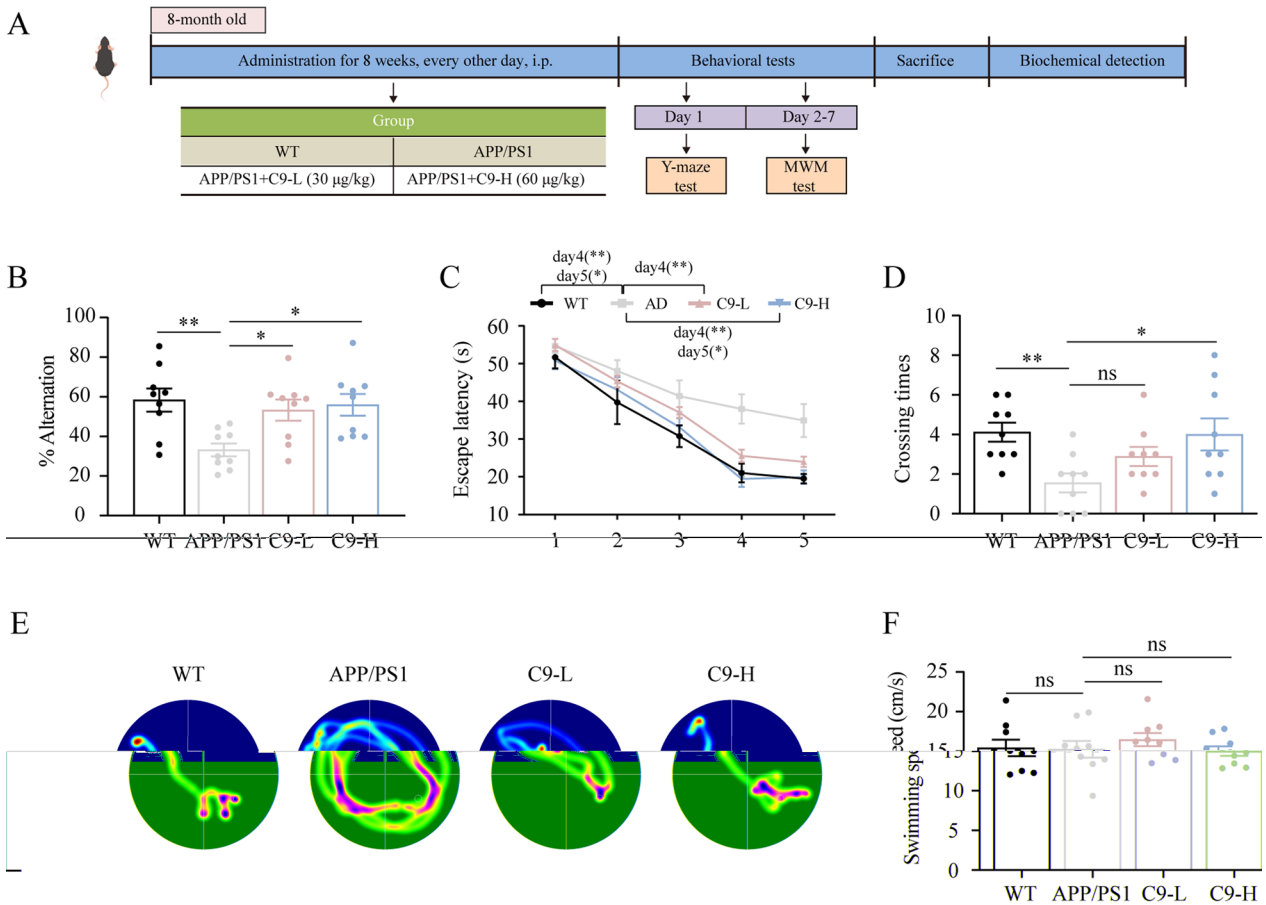

Fig. 2 Chemerin-9 ameliorates cognitive deficits in APP/PS1 mice. **A** Schematic diagram of the experimental procedure. **B** The percentage of alternation ($n=9$). **C** The escape latency in the navigation trials of the hidden platform task ($n=9$). **D** Frequency of platform crossing in the probe trial ($n=9$). **E** Representative path tracings during the navigation trials. **F** Swimming speed in the probe trial ($n=9$). *$P<0.05$; **$P<0.01$. C9-H = High dose of chemerin-9; C9-L = Low dose of chemerin-9

Chemerin-9 attenuates neuronal damage and synaptic impairment in APP/PS1 mice

Degeneration and loss of neurons in the brain are well-known contributors to cognitive impairment in AD. Therefore, we used NeuN and Nissl staining to observe the number and morphological changes in neurons after treatment with chemerin-9. As depicted in Fig. 3A and B, NeuN-positive cells in the hippocampus and cortex of APP/PS1 mice were not significantly different from the WT mice and chemerin-9 treated mice. IHC analysis of Nissl staining revealed that the cortical and hippocampal neurons of the WT mice exhibited copious and sizable Nissl bodies. In contrast, the number of Nissl-positive neurons in the cortex and hippocampus of the APP/PS1 mice was reduced, and the affected neurons exhibited shrinkage, along with hyperchromatic nuclei and sparse Nissl bodies. Following the treatment with chemerin-9, the loss of Nissl-positive neurons was less pronounced (Fig. 3C and D). Dystrophic neurites showed swollen abnormal morphology, and were abundant in the vicinity of Aβ deposits in the brains of AD mice. To further investigate the effects of chemerin-9 on neuronal pathology, we analysed LAMP1 as a marker of dystrophic neurites. We observed an increase of LAMP1-positive areas in the hippocampus and cortex of APP/PS1 mice as campare with WT mice, while chemerin-9 reversed the dystrophic neurites in APP/PS1 mice (Fig. 3E and F). Cognitive decline is closely correlated with synaptic impairment in the hippocampus [24]. Hence, we employed Golgi staining to evaluate the effects of chemerin-9 on dendritic morphology. As shown in Fig. 3G and H, the number of dendritic spines in APP/PS1 mice was found to be significantly lower than that of WT mice. However, the administration of chemerin-9 at either low or high doses to APP/PS1 mice resulted in a marked increase in the number of dendritic spines when compared to untreated APP/PS1 mice. Moreover, we performed western blot to assess the effects of chemerin-9 on the synapse-related proteins SYN and PSD95 in the hippocampus of APP/PS1 mice. The results demonstrated that the relative levels of SYN and PSD95 were considerably lower in the APP/PS1 mice in comparison to those in the WT mice. However, the administration of either low or high doses of chemerin-9 resulted in the reversal of this effect (Fig. 3I and J). Taken together, these findings indicate that the administration of chemerin-9 ameliorates neuronal damage and synaptic dysfunction in APP/PS1 mice.

Chemerin-9 relieves Aβ burden in APP/PS1 mice

The accumulation of Aβ and deposition of plaques have been proposed to induce synaptic impairment and neuronal death, resulting in cognitive decline in APP/PS1 mice [25]. To determine whether the rescued cognitive function by chemerin-9 was associated with the alteration of Aβ load, Thioflavin-S and 6E10 co-staining were performed. As shown in Fig. 4A-D, Thioflavin-S and 6E10 co-staining revealed that amyloid plaques were obvious in the hippocampus and cortex of APP/PS1 mice, whereas the areas covered by amyloid plaques were significantly lower after chemerin-9 treatment. Moreover, ELISA assays were performed to measure the levels of $A\beta_{1-40}$ and $A\beta_{1-42}$, the primary C-terminal variants of the Aβ protein that constitute the majority of Aβ plaques, in the hippocampus and cortex of APP/PS1 mice treated with chemerin-9. As shown in Fig. 4E, although the levels of $A\beta_{1-40}$ showed a decreasing trend, no significant differences were observed in the hippocampus and cortex of APP/PS1 mice following chemerin-9 treatment. However, the levels of $A\beta_{1-42}$ in the hippocampus and cortex of APP/PS1 mice were dramatically lowered through the administration of either a low or high dose of chemerin-9 (Fig. 4F). Altogether, the results demonstrate that chemerin-9 effectively relieves Aβ burden in APP/PS1 mice.

Chemerin-9 facilitates microglia-mediated Aβ phagocytosis

To further elucidate the potential mechanisms that contribute to the phenotype observed in APP/PS1 mice treated with chemerin-9, we undertook transcriptomic analysis on the hippocampi of both chemerin-9-treated and vehicle-treated APP/PS1 mice. The results showed that a total of 33 genes were upregulated and 11 genes were downregulated (Fig. 5A). The KEGG analysis performed on the combined DEGs in chemerin-9-treated and vehicle-treated APP/PS1 mice revealed that several pathways were considerably influenced. Specifically, the phagosome, NOD-like

(See figure on next page.)

Fig. 3 Chemerin-9 attenuates neuronal damage and synaptic impairment in APP/PS1 mice. **A** Representative NeuN staining images in the hippocampus and cortex. **B** Quantification of the area of NeuN staining within the hippocampus and cortex ($n=4$). **C** Representative Nissl staining images in the hippocampus and cortex. **D** Quantification of Nissl-positive cells within the hippocampus and cortex ($n=4$). **G** Representative images of neuronal dendrites by Golgi staining. **C** The quantification of the spine density ($n=3$). **D** Representative immunoblotting bands of SYN and PSD95 in the hippocampus. **E** Quantitative analysis of SYN/actin and PSD95/actin ($n=3$). *$P<0.05$; **$P<0.01$; ***$P<0.001$. SYN = synaptophysin; C9-H = High dose of chemerin-9; C9-L = Low dose of chemerin-9

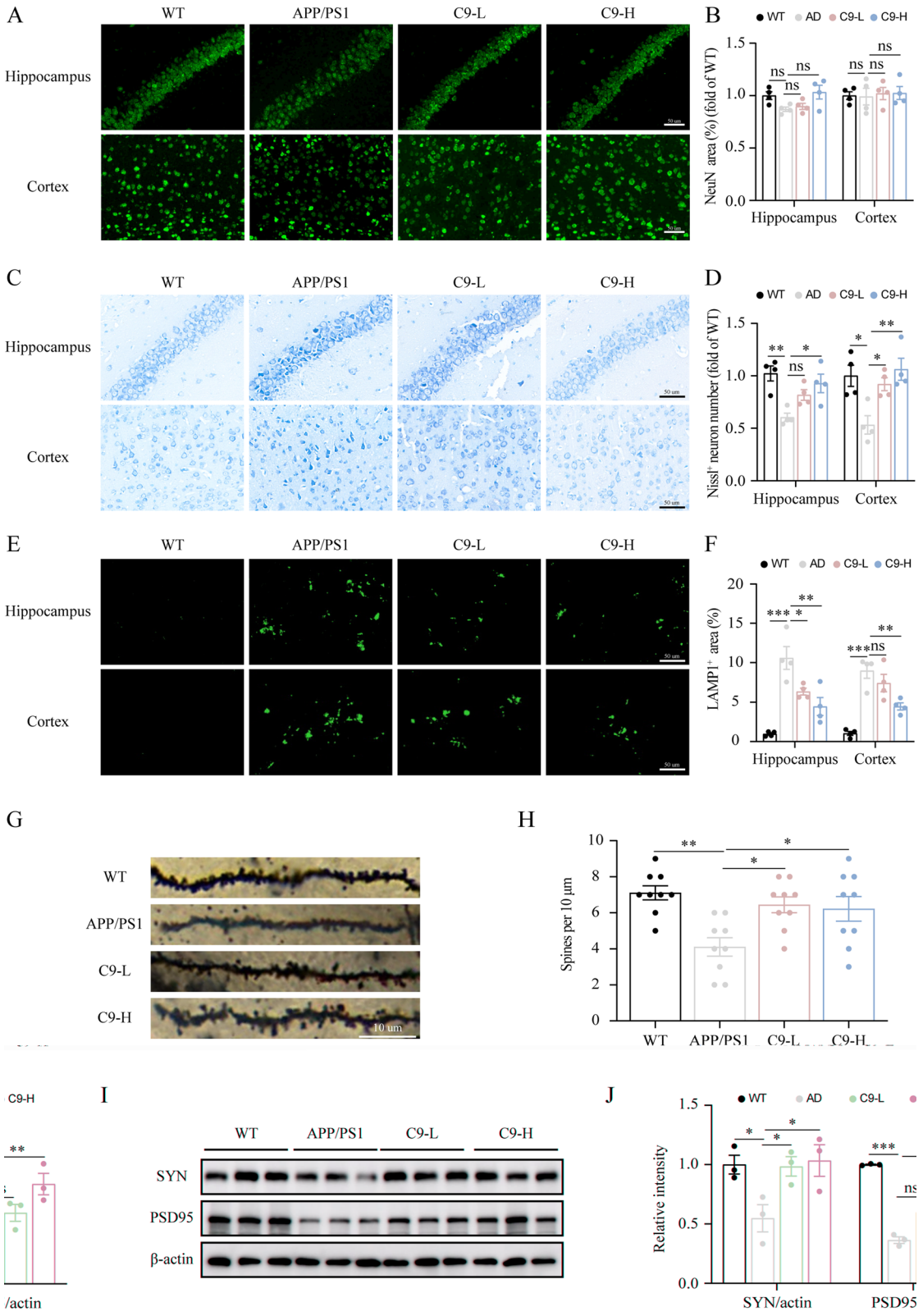

Fig. 3 (See legend on previous page.)

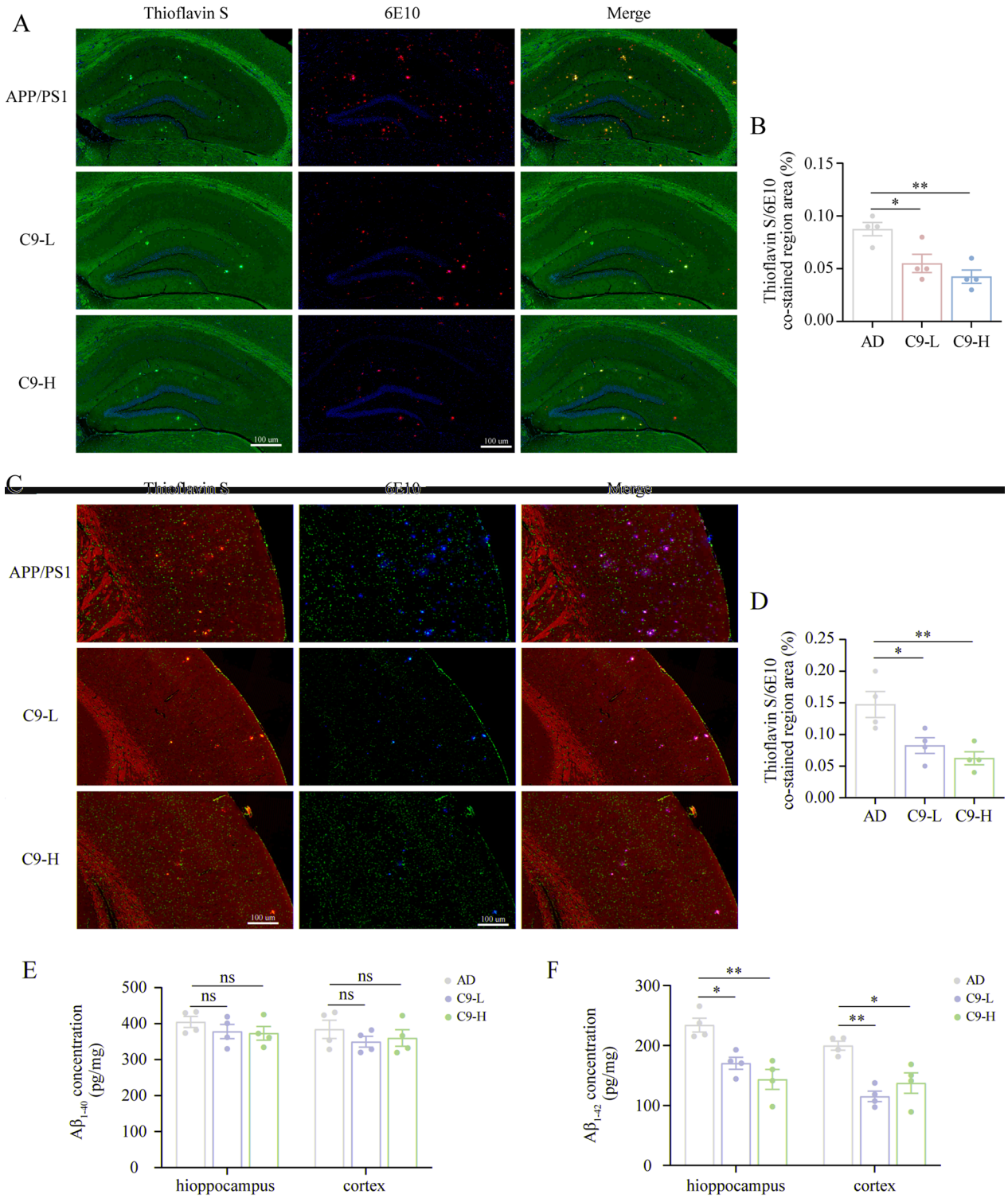

Fig. 4 Chemerin-9 relieves Aβ burden in APP/PS1 mice. **A** IHC staining of amyloid plaques with thioflavin S and 6E10 in the hippocampus. **B** Quantification of thioflavin S and 6E10 co-stained area in the hippocampus ($n=4$). **C** IHC staining of amyloid plaques with thioflavin S and 6E10 in the cortex. **D** Quantification of thioflavin S and 6E10 co-stained area in the cortex ($n=4$). **E** ELISA was performed to detect the concentration of $A\beta_{1-40}$ ($n=4$). **F** ELISA was performed to detect the concentration of $A\beta_{1-42}$ ($n=4$). *$P<0.05$; **$P<0.01$; ***$P<0.001$. C9-H = High dose of chemerin-9; C9-L = Low dose of chemerin-9

receptor signaling pathway, TNF signaling pathway, and neuroactive ligand-receptor interaction pathways were among the most affected (Fig. 5B). Moreover, we calculated the normalized enrichment score (NES) using GSEA and identified two gene sets that were significantly enriched: protein digestion and absorption and the NOD-like receptor signaling pathway (Fig. 5C and D).

It has been well established that the accumulation of Aβ is predominantly caused by an imbalance in the production and elimination of Aβ. Our bulk transcriptomic results suggested that the administration of chemerin-9 led to alterations in genes associated with phagocytosis (Fig. 5B and C), including Clec7a (Fig. 5A), which plausibly facilitated the reduction of Aβ by enhancing clearance. Microglia are known to play a pivotal role in regulating the clearance and degradation of Aβ [26]. Thus, to explore the potential of microglia surrounding the plaques to engulf Aβ and facilitate Aβ clearance, we performed co-immunostaining of Iba1, Clec7a, and 6E10, which are established markers for microglia, disease-associated microglial marker, and Aβ, respectively. We observed no statistically significant difference in the number of microglia surrounding Aβ plaques between the chemerin-9-treated APP/PS1 mice and the vehicle-treated APP/PS1 mice (Fig. 5E and F). However, we found that the microglia in the APP/PS1 mice treated with chemerin-9 demonstrated a significant upregulation in Clec7a expression compared to the microglia in the vehicle-treated APP/PS1 mice, suggesting that chemerin-9 facilitated the clearance and phagocytosis of Aβ by the microglia (Fig. 5E and G). Additionally, we sought to determine whether the accumulation of Aβ was a consequence of an increase in Aβ production. However, there were no significant changes in the levels of APP or enzymes related to Aβ metabolism, including BACE1, PS1, PEN2, and Nicastrin (Fig. 5H and I). Taken together, these results suggest that the lower level of Aβ accumulation in the chemerin-9-treated APP/PS1 mice is associated with increased Aβ phagocytosis.

Chemerin-9 inhibits microglial NLRP3 inflammasome activation

Based on the results from both the KEGG and GSEA analyses, the NOD-like receptor signaling pathway was one of the most affected pathways (Fig. 5B and D). Moreover, the NLRP3 inflammasome, which is the most common form of inflammasome, has been implicated in numerous chronic inflammatory disorders due to its capacity to sense inflammatory crystals and aggregated proteins, such as Aβ [27, 28]. Therefore, we investigated whether the microglial NLRP3 inflammasome was altered by chemerin-9 in APP/PS1 mice. As shown in Fig. 6A and B, the APP/PS1 mice exhibited a marked increase in the expression of NLRP3, ASC, and active caspase1 levels as compared to the WT mice. Remarkably, treatment with chemerin-9 was found to effectively inhibit the activation of the NLRP3/ASC/caspase1 axis (Fig. 6A and B). Consistently, immunofluorescence staining indicated the activation of microglial NLRP3 inflammasome in the hippocampus of APP/PS1 mice, as evidenced by a significantly increased fluorescence intensity of NLRP3 in Iba1-positive cells (Fig. 6C and D). Treatment with chemerin-9 led to a marked decrease in the fluorescence intensity of NLRP3 in Iba1-positive cells (Fig. 6C and D). Furthermore, ELISA results revealed that APP/PS1 mice expressed significantly higher levels of IL-1β and IL-6 compared to WT mice, while APP/PS1 mice receiving chemerin-9 showed a noticeable reversal of these changes (Fig. 6E and F). These findings indicate that the cognitive benefits of chemerin-9 in AD may be due in part to its ability to inhibit microglial NLRP3 inflammasome activation and lower cytokine levels.

Chemerin-9 modulates microglial phagocytosis and attenuates microglia-mediated neuroinflammation in a ChemR23-dependent manner

To investigate whether chemerin-9 affects microglial function through ChemR23, primary microglia were treated with chemerin-9 and the ChemR23 inhibitor α-NETA after $A\beta_{42}$ oligomers treatment. The results showed that chemerin-9-treated microglia had a greater phagocytic capacity than control and Aβ-treated microglia, as demonstrated by the increased uptake of HiLyte™

(See figure on next page.)

Fig. 5 Disease-associated microglial marker is regulated by Chemerin-9. **A** Numbers of genes that were upregulated or downregulated and the volcano plot of DEGs between the chemerin-9-treated APP/PS1 mice versus the vehicle-treated APP/PS1 mice. **B** Bubble chart showing significant enrichment of DEGs in various pathways. **C** GSEA of protein digestion and absorption pathway of chemerin-9-treated APP/PS1 mice versus vehicle-treated APP/PS1 mice. **D** GSEA of the NOD-like receptor signaling pathway of chemerin-9-treated APP/PS1 mice versus vehicle-treated APP/PS1 mice. **E** Immunofluorescent staining of Iba1, Clec7a, and 6E10 in the hippocampus. **F** Quantification of Iba1-positive cell number within 15 μm radius distance around the Aβ plaque ($n = 3$). **G** Percentage of Clec7a and Iba1-positive area versus Aβ plaque area ($n = 3$). **H** Representative immunoblotting bands of APP, BACE1, PS1, PEN2, and Nicastrin in the hippocampus. **I** Quantitative analysis of APP/actin, BACE1/actin, PS1/actin, PEN2/actin, and Nicastrin/actin ($n = 3$). *$P < 0.05$. PS1 = Presenilin 1; C9-H = High dose of chemerin-9; C9-L = Low dose of chemerin-9

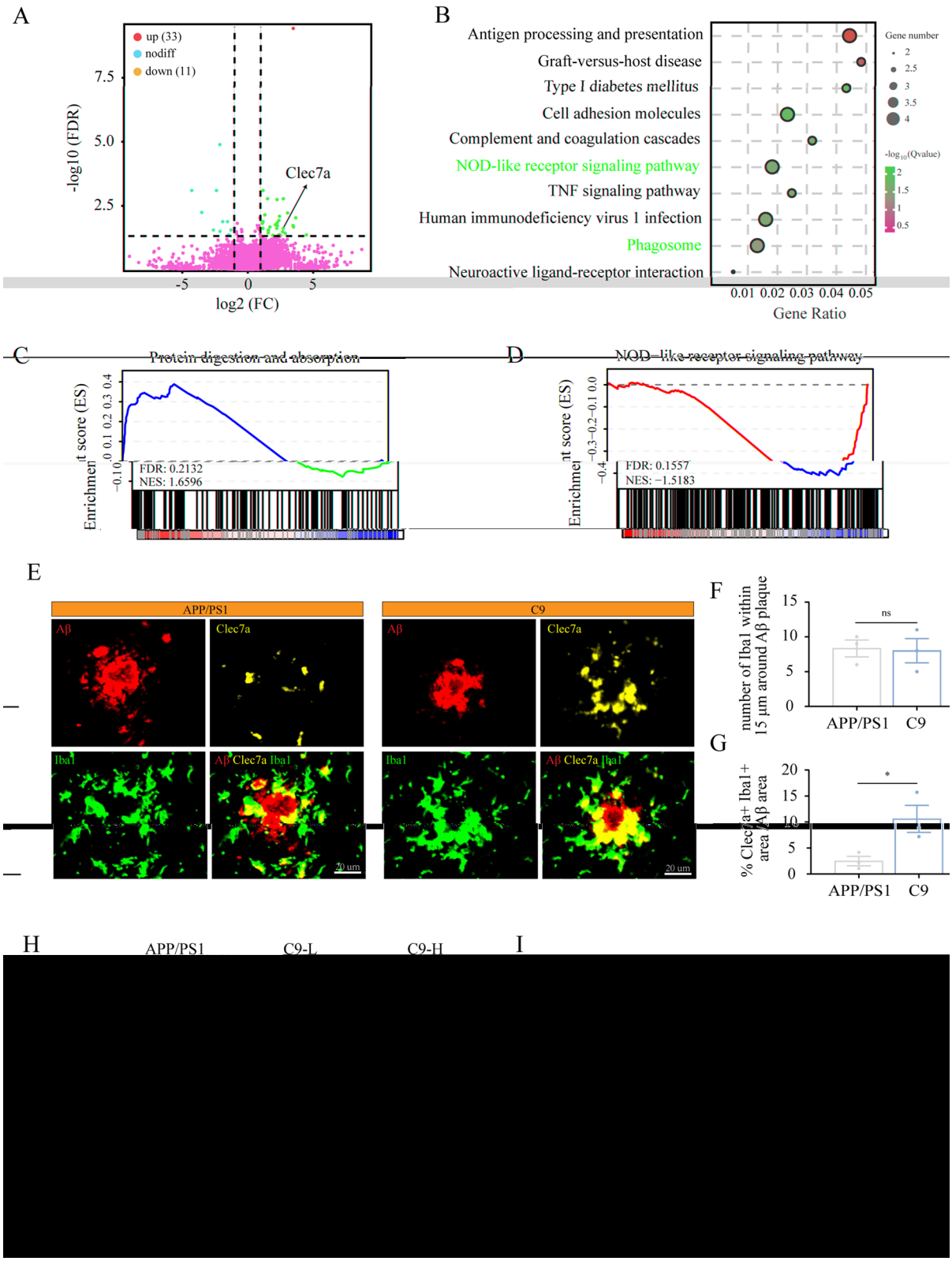

Fig. 5 (See legend on previous page.)

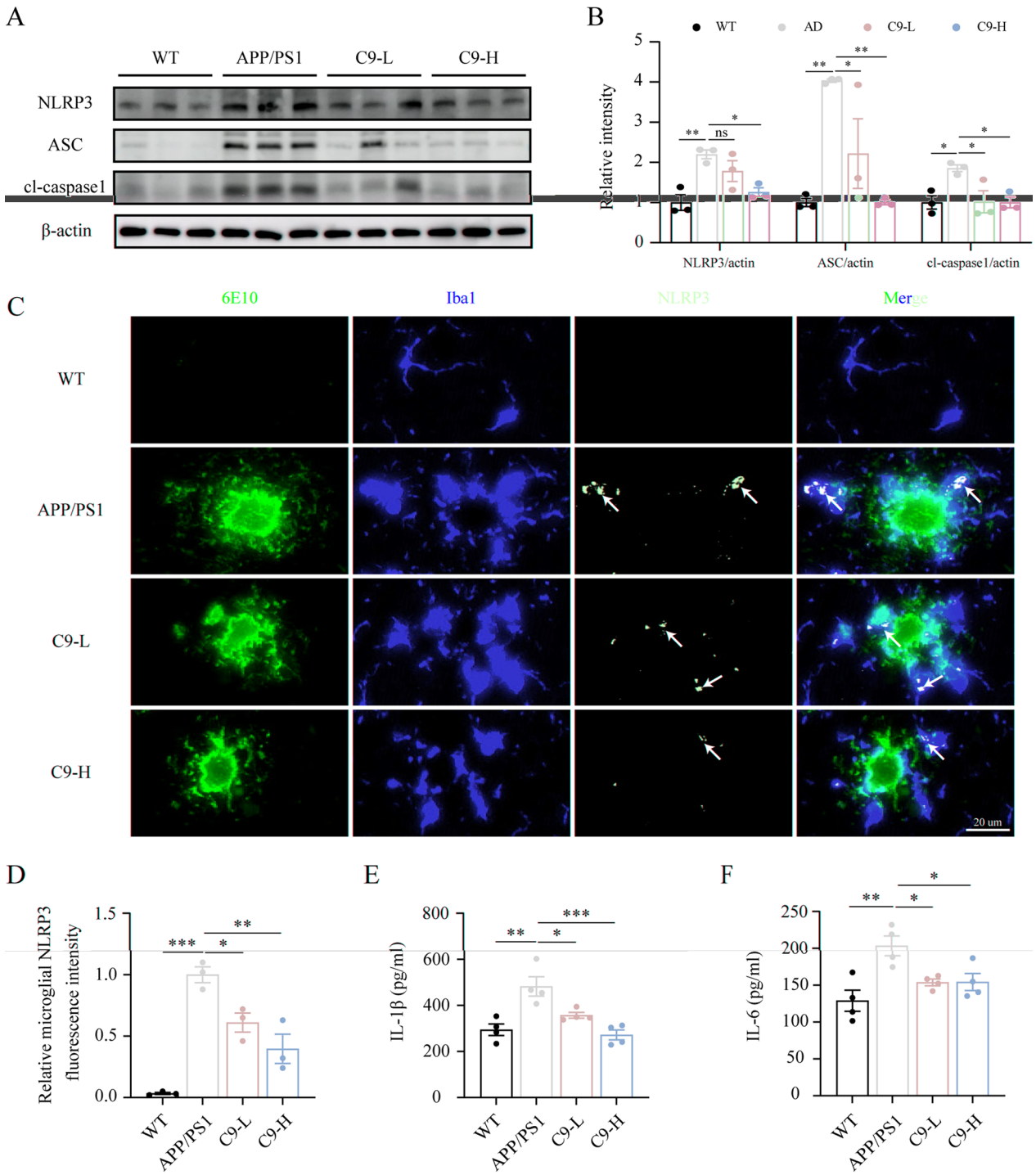

Fig. 6 Chemerin-9 inhibits microglial NLRP3 inflammasome activation. **A** Representative immunoblotting bands of NLRP3, ASC, and cl-caspase1 in the hippocampus. **B** Quantitative analysis of NLRP3/actin, ASC/actin, and cl-caspase1/actin ($n=3$). **C** Immunofluorescent staining of NLRP3 and Iba1. **D** Relative NLRP3 fluorescence intensity in Iba1-positive cells ($n=3$). **E**, **F** ELISA was performed to detect the concentration of IL-1β and IL-6 ($n=4$). $^{*}P<0.05$; $^{**}P<0.01$; $^{***}P<0.001$. C9-H = High dose of chemerin-9; C9-L = Low dose of chemerin-9

Fluor labeled $A\beta_{1-42}$ peptide. On the other hand, the HiLyte™ Fluor labeled $A\beta_{1-42}$ peptide uptake decreased in the α-NETA-treated group (Fig. 7A and B). In addition, we found that the increased levels of NLRP3, ASC, and cl-caspase1 and the subsequent pro-inflammatory cytokines (including IL-6 and TNF-α) in the Aβ-treated group were downregulated after treatment with chemerin-9. However, α-NETA treatment reversed the above changes (Fig. 7C-F). To determine whether the effect of chemerin-9 on microglia phenotype would have a subsequent impact on neuronal survival, we treated primary neurons with the supernatant collected from conditional microglia culture. The results of live-dead staining assays showed that chemerin-9 rescued the $A\beta_{42}$-induced decline of cell viability. Nevertheless, administration with α-NETA abrogated the neuroprotective effects of chemerin-9 (Fig. 7G). Overall, the data above suggest that chemerin-9, by interacting with ChemR23, modulates microglial phagocytosis and mitigates microglia-associated neuroinflammation, ultimately serving a neuroprotective role in AD.

Discussion

For more than a hundred years, AD has been one of the most researched neurodegenerative diseases. Even though multiple theories have been proposed, the actual cause remains unknown, thus leaving few viable treatments. Here we document that the levels of chemerin and its receptor, ChemR23 are increased in microglia in AD patients and APP/PS1 mice. Elevated levels of chemerin, which is considered as an adipocytokine, have been correlated with obesity, insulin resistance, metabolic syndrome, and inflammation [9, 29]. However, the effect of chemerin/ChemR23 on microglia function and its involvement in the development of AD is yet to be determined. Thus, we used chemerin-9, a bioactive nonapeptide derived from full-length chemerin to intervene in AD mice [13]. Our results demonstrated the therapeutic efficacy of chemerin-9 for AD in APP/PS1 mice, as evidenced by the recovery of spatial learning and memory, the decrease in Aβ deposition, and the prevention of synaptic loss. Similarly, our recent research found that chemerin-9 ameliorates the cognitive impairment and synaptic loss of diabetic mice [19]. Collectively, our findings shed some light on the role of chemerin in the etiology of cognitive impairment, suggesting that boosting chemerin signaling could be a potential therapy for AD.

Increasing evidence indicates that microglia, the predominant immune cells and professional phagocytes of the central nervous system, play an essential role in the pathogenesis and progression of AD by modulating inflammatory responses and phagocytosis of Aβ [7, 30]. Indeed, recent genome-wide association studies have uncovered many genetic loci that are linked to the risk of AD, mostly related to the immune functions of microglia or the neuroinflammatory response [31, 32]. Moreover, a novel type of microglia, referred to as 'disease-associated microglia', was identified by single-cell sorting and sequencing in a mouse model of AD and was then corroborated by postmortem brain samples of AD patients, suggesting that microglia have a much more intricate role in AD than previously assumed [33]. Disease-associated microglia may play a role in containing Aβ plaques and slowing disease progression. Recent studies have shown that Clec7a is upregulated during the transition from homeostatic microglia to disease-associated microglia, which are commonly around Aβ plaques in AD [34]. Additionally, research indicates that the chemerin/ChemR23 axis is involved in the migration and recruitment of microglia to senile plaques through the p38 MAPK pathway [35]. In the present study, it was observed that levels of microglial Clec7a were higher around Aβ plaques in chemerin-9-treated APP/PS1 mice compared to vehicle-treated APP/PS1 mice, suggesting an intensified microglial response to amyloid pathology following chemerin-9 treatment. Moreover, Zhang et al. reported that human recombinant chemerin ameliorates the germinal matrix hemorrhage-induced inflammatory response by promoting the ChemR23/CAMKK2/AMPK/Nrf2 pathway in microglia [36]. In the present study, our findings revealed that chemerin-9 treatment decreases microglial NLRP3 inflammasome activation and reduces the production of inflammatory cytokines. Our results above indicate that sufficient chemerin signaling can shift microglia towards a plaque-associated phenotype, rebalancing their phagocytosis and immune actions.

(See figure on next page.)

Fig. 7 Chemerin-9 modulates microglial phagocytosis and attenuates microglia-mediated neuroinflammation in a ChemR23-dependent manner. **A**, **B** After incubation with HiLyte™ Fluor 488-labeled $A\beta_{1-42}$, cells were imaged and the total amount of fluorescence within primary microglia was quantified ($n = 3$). **C** Representative immunoblotting bands of NLRP3, ASC, and cl-caspase1 in the primary microglia. **D** Quantitative analysis of NLRP3/actin, ASC/actin, and cl-caspase1/actin ($n = 3$). **E**, **F** ELISA was performed to detect the concentration of IL-6 and TNF-α ($n = 4$). (G) Fluorescence images of primary neurons stained with calcein AM (live cells, green fluorescence) and PI (dead cells, red fluorescence) after different treatments ($n = 3$). $^{*}P < 0.05$; $^{**}P < 0.01$; $^{***}P < 0.001$. C9 = chemerin-9

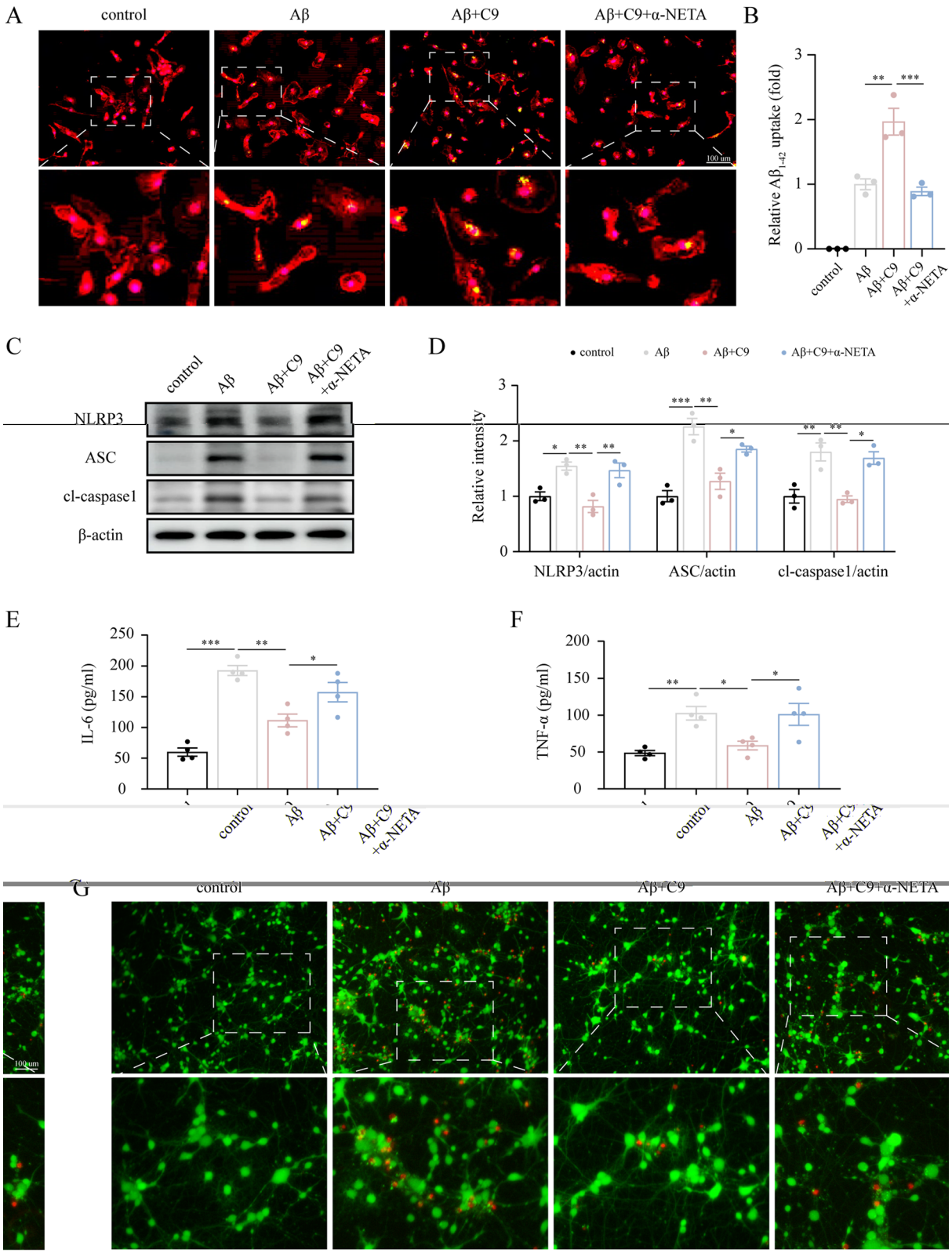

Fig. 7 (See legend on previous page.)

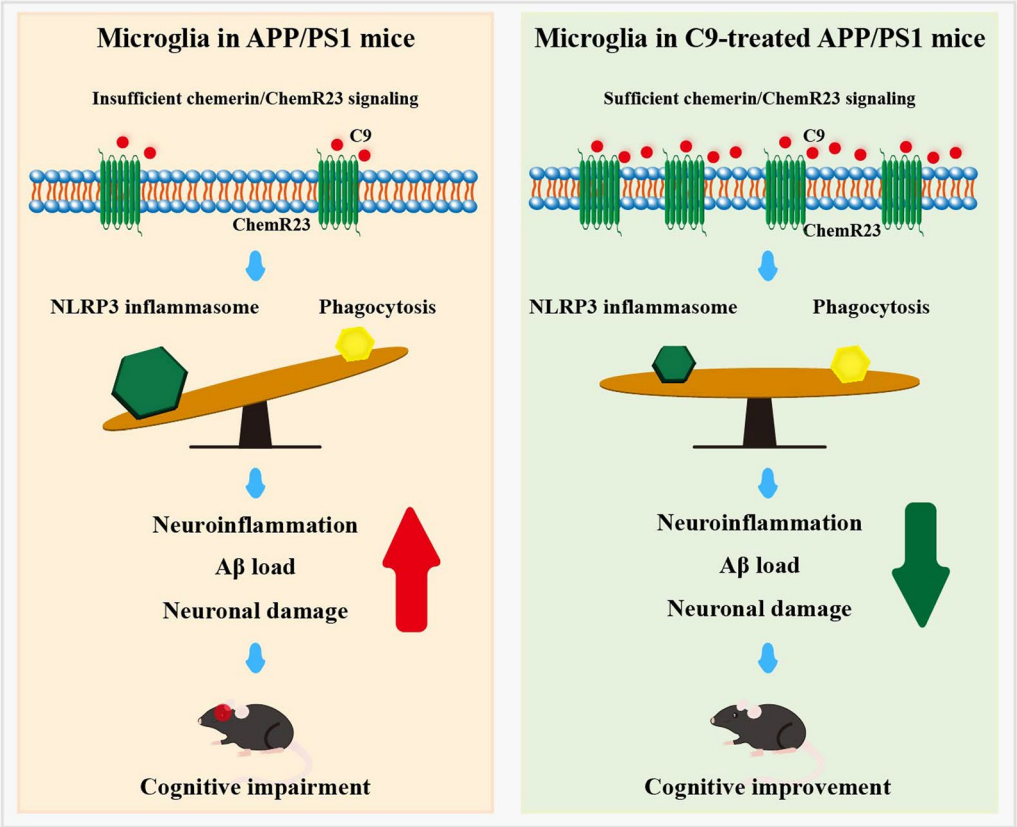

Fig. 8 Graphical abstract

The molecular mechanisms of chemerin signaling in AD are of further interest. Analysis of RNAseq data revealed that the NOD-like receptor signaling pathway was among the most impacted pathways. The NLRP3 inflammasome, which is the most common one in the NOD-like receptor signaling pathway, has been extensively studied in relation to AD. Studies have shown that NLRP3 deficiency or impairment of its essential signaling components leads to a decrease in Aβ-induced microglial activation in vitro [37], Aβ accumulation, Tau pathology, and cognitive decline in AD mouse models [27, 38]. And a growing body of studies has indicated that chemerin/ChemR23 interacts with NLRP3 and regulates its activation. For example, Liang et al. reported that aggregation of chemerin could lead to microglia recruitment, activation of NLRP3, release of inflammatory cytokines, and cognitive impairment in the offspring of mothers with diabetes in a ChemR23-dependent manner [39]. In addition, a study has shown that the chemerin/ChemR23 axis promotes inflammation and pyroptosis by activating NLRP3 Inflammasome in diabetic cardiomyopathy rats [40]. In line with previous studies, we observed increased NLRP3 inflammasome activation and proinflammatory cytokine production in Aβ-induced primary microglia and APP/PS1 mice. Nevertheless, treatment with chemerin-9 significantly reversed these changes both in vitro and in vivo. Dual regulatory effects of chemerin on inflammation, as seen in our and previous studies, may be linked to the physiological context and stage of the disease. Our further in vitro investigation showed that the anti-inflammatory effects of chemerin-9 were almost completely abrogated by the ChemR23 inhibitor α-NETA, suggesting that the beneficial effects of chemerin-9 were ChemR23-dependent.

In summary, our study demonstrate that chemerin-9 ameliorates cognitive deficits in APP/PS1 transgenic mice by boosting a disease-associated microglial response via modulating phagocytosis and attenuating NLRP3 inflammasome activation in a ChemR23-dependent manner (Fig. 8).

Collectively, our work presents chemerin-9 as a novel therapeutic candidate against AD.

Abbreviations

AD	Alzheimer's disease
RARRES2	Retinoic acid receptor responder 2 protein
Aβ	Amyloid beta
MWM	Morris water maze
ISH	In situ hybridization
RNAseq	RNA Sequencing

PS1	Presenilin 1
SYN	Synaptophysin
PSD95	Postsynaptic density protein-95
NLRP3	Nucleotide-binding oligomerization domain-like receptor protein 3
ASC	Apoptosis-associated speck-like protein containing a CARD

Supplementary Information

The online version contains supplementary material available at https://doi.org/10.1186/s12974-024-03325-y.

Supplementary Material 1.

Supplementary Material 2.

Acknowledgements
Not applicable.

Author contributions
X.W. and J.Z. conceived and designed the study. X.W. and Y.Z. (Yuwu Zhao) supervised the research. J.Z., Y.Z. (Yaxuan Zhang), X.Z. (Xiaojie Zhang), J.D., F.Z., and Q.L. performed experiments and analyzed the data. L.L., X.Z. (Xue Zheng), and M.Z. were involved in animal modeling and data analysis. B.F. provided critical suggestions for the study. J.Z. and X.W. draft the manuscript.

Funding
This study was supported by research grants from the National Natural Science Foundation of China (Grant No. 81974158 and 82071288) and Health science and technology project of Fujian Province (Grant No. 2024QNB012).

Data availability
The data that support the findings of this study are available within the article and from the corresponding authors upon reasonable request.

Declarations

Ethics approval and consent to participate
All procedures were authorized by the ethical committee on animal welfare of Shanghai Sixth People's Hospital Affiliated to Shanghai Jiao Tong University School of Medicine.

Consent for publication
All of the authors approved the final version for publication.

Competing interests
The authors declare no competing interests.

Author details
[1]Department of Neurology, Shanghai Sixth People's Hospital, Shanghai Jiao Tong University School of Medicine, Yishan Road 600, Shanghai 200233, China. [2]Department of Neurology, The First Affiliated Hospital of Xiamen University, School of Medicine, Xiamen University, Xiamen, China. [3]Shanghai Neurological Rare Disease Biobank and Precision Diagnostic Technical Service Platform, Shanghai, China. [4]Department of Neurology, The Second People's Hospital of Lianyungang, Lianyungang, Jiangsu, China.

Received: 13 October 2023 Accepted: 16 December 2024
Published online: 08 January 2025

References

1. Scheltens P, De Strooper B, Kivipelto M, Holstege H, Chetelat G, Teunissen CE, Cummings J, van der Flier WM. Alzheimer's disease. Lancet. 2021;397(10284):1577–90.
2. Li X, Ospitalieri S, Robberechts T, Hofmann L, Schmid C, Rijal Upadhaya A, Koper MJ, von Arnim CAF, Kumar S, Willem M, Gnoth K, Ramakers M, Schymkowitz J, Rousseau F, Walter J, Ronisz A, Balakrishnan K, Thal DR. Seeding, maturation and propagation of amyloid beta-peptide aggregates in Alzheimer's disease. Brain. 2022;145(10):3558–70.
3. Smirnov D, Galasko D. Dynamics of neuroinflammation in Alzheimer's disease. Lancet Neurol. 2022;21(4):297–8.
4. Calsolaro V, Edison P. Neuroinflammation in Alzheimer's disease: current evidence and future directions. Alzheimers Dement. 2016;12(6):719–32.
5. Ennerfelt H, Frost EL, Shapiro DA, Holliday C, Zengeler KE, Voithofer G, Bolte AC, Lammert CR, Kulas JA, Ulland TK, Lukens JR. SYK coordinates neuroprotective microglial responses in neurodegenerative disease. Cell. 2022;185(22):4135-4152 e22.
6. De Schepper S, Ge JZ, Crowley G, Ferreira LSS, Garceau D, Toomey CE, Sokolova D, Rueda-Carrasco J, Shin SH, Kim JS, Childs T, Lashley T, Burden JJ, Sasner M, Sala Frigerio C, Jung S, Hong S. Perivascular cells induce microglial phagocytic states and synaptic engulfment via SPP1 in mouse models of Alzheimer's disease. Nat Neurosci. 2023;26(3):406–15.
7. Sarlus H, Heneka MT. Microglia in Alzheimer's disease. J Clin Invest. 2017;127(9):3240–9.
8. Li L, Wu XH, Zhao XJ, Xu L, Pan CL, Zhang ZY. Zerumbone ameliorates behavioral impairments and neuropathology in transgenic APP/PS1 mice by suppressing MAPK signaling. J Neuroinflammation. 2020;17(1):61.
9. Ernst MC, Sinal CJ. Chemerin: at the crossroads of inflammation and obesity. Trends Endocrinol Metab. 2010;21(11):660–7.
10. Pelczynska M, Mikulska AA, Czyzewska K, Bogdanski P, Grzelak T. The association of serum circulating neuropeptide Q and chemerin levels with cardiometabolic risk factors among patients with metabolic syndrome. Biomolecules. 2021;11(12):1863.
11. Mariani F, Roncucci L. Chemerin/chemR23 axis in inflammation onset and resolution. Inflamm Res. 2015;64(2):85–95.
12. Rourke JL, Dranse HJ, Sinal CJ. Towards an integrative approach to understanding the role of chemerin in human health and disease. Obes Rev. 2013;14(3):245–62.
13. Zhang X, Weiss T, Cheng MH, Chen S, Ambrosius CK, Czerniak AS, Li K, Feng M, Bahar I, Beck-Sickinger AG, Zhang C. Structural basis of CMKLR1 signaling induced by chemerin9, bioRxiv. 2023.
14. Sato K, Yoshizawa H, Seki T, Shirai R, Yamashita T, Okano T, Shibata K, Wakamatsu MJ, Mori Y, Morita T, Matsuyama TA, Ishibashi-Ueda H, Hirano T, Watanabe T. Chemerin-9, a potent agonist of chemerin receptor (ChemR23), prevents atherogenesis. Clin Sci. 2019;133(16):1779–96.
15. Abareshi A, Momenabadi S, Vafaei AA, Bandegi AR, Vakili A. Neuroprotective effects of Chemerin on a mouse stroke model: behavioral and molecular dimensions. Neurochem Res. 2021;46(12):3301–13.
16. Graham KL, Zabel BA, Loghavi S, Zuniga LA, Ho PP, Sobel RA, Butcher EC. Chemokine-like receptor-1 expression by central nervous system-infiltrating leukocytes and involvement in a model of autoimmune demyelinating disease. J Immunol. 2009;183(10):6717–23.
17. Duraes FV, Lippens C, Steinbach K, Dubrot J, Brighouse D, Bendriss-Vermare N, Issazadeh-Navikas S, Merkler D, Hugues S. pDC therapy induces recovery from EAE by recruiting endogenous pDC to sites of CNS inflammation. J Autoimmun. 2016;67:8–18.
18. Graham KL, Zhang JV, Lewen S, Burke TM, Dang T, Zoudilova M, Sobel RA, Butcher EC, Zabel BA. A novel CMKLR1 small molecule antagonist suppresses CNS autoimmune inflammatory disease. PLoS ONE. 2014;9(12):e112925.
19. Zhang J, Liu L, Zhang Y, Yuan Y, Miao Z, Lu K, Zhang X, Ni R, Zhang H, Zhao Y, Wang X. ChemR23 signaling ameliorates cognitive impairments in diabetic mice via dampening oxidative stress and NLRP3 inflammasome activation. Redox Biol. 2022;58:102554.
20. Zhang M, Qian C, Zheng ZG, Qian F, Wang Y, Thu PM, Zhang X, Zhou Y, Tu L, Liu Q, Li HJ, Yang H, Li P, Xu X. Jujuboside A promotes Abeta clearance and ameliorates cognitive deficiency in Alzheimer's disease through activating Axl/HSP90/PPARgamma pathway. Theranostics. 2018;8(15):4262–78.
21. Zhang H, Wang H, Gao F, Yang J, Xu Y, Fu Y, Cai M, Zhang X, Yang Q, Tong K, Hu Y, Chen H, Ma C, He W, Zhang J. TSPO deficiency accelerates amyloid pathology and neuroinflammation by impairing microglial phagocytosis. Neurobiol Aging. 2021;106:292–303.
22. Machlovi SI, Neuner SM, Hemmer BM, Khan R, Liu Y, Huang M, Zhu JD, Castellano JM, Cai D, Marcora E, Goate AM. APOE4 confers transcriptomic and functional alterations to primary mouse microglia. Neurobiol Dis. 2022;164:105615.

23. Spangenberg E, Severson PL, Hohsfield LA, Crapser J, Zhang J, Burton EA, Zhang Y, Spevak W, Lin J, Phan NY, Habets G, Rymar A, Tsang G, Walters J, Nespi M, Singh P, Broome S, Ibrahim P, Zhang C, Bollag G, West BL, Green KN. Sustained microglial depletion with CSF1R inhibitor impairs parenchymal plaque development in an Alzheimer's disease model. Nat Commun. 2019;10(1):3758.
24. Neves G, Cooke SF, Bliss TV. Synaptic plasticity, memory and the hippocampus: a neural network approach to causality. Nat Rev Neurosci. 2008;9(1):65–75.
25. Fu AK, Hung KW, Huang H, Gu S, Shen Y, Cheng EY, Ip FC, Huang X, Fu WY, Ip NY. Blockade of EphA4 signaling ameliorates hippocampal synaptic dysfunctions in mouse models of Alzheimer's disease. Proc Natl Acad Sci U S A. 2014;111(27):9959–64.
26. Singh N, Das B, Zhou J, Hu X, Yan R. Targeted BACE-1 inhibition in microglia enhances amyloid clearance and improved cognitive performance. Sci Adv. 2022;8(29):eabo3610.
27. Heneka MT, Kummer MP, Stutz A, Delekate A, Schwartz S, Vieira-Saecker A, Griep A, Axt D, Remus A, Tzeng TC, Gelpi E, Halle A, Korte M, Latz E, Golenbock DT. NLRP3 is activated in Alzheimer's disease and contributes to pathology in APP/PS1 mice. Nature. 2013;493(7434):674–8.
28. Martinon F, Mayor A, Tschopp J. The inflammasomes: guardians of the body. Annu Rev Immunol. 2009;27:229–65.
29. Chakaroun R, Raschpichler M, Kloting N, Oberbach A, Flehmig G, Kern M, Schon MR, Shang E, Lohmann T, Dressler M, Fasshauer M, Stumvoll M, Bluher M. Effects of weight loss and exercise on chemerin serum concentrations and adipose tissue expression in human obesity. Metabolism. 2012;61(5):706–14.
30. Lee CYD, Daggett A, Gu X, Jiang LL, Langfelder P, Li X, Wang N, Zhao Y, Park CS, Cooper Y, Ferando I, Mody I, Coppola G, Xu H, Yang XW. Elevated TREM2 gene dosage reprograms Microglia Responsivity and ameliorates pathological phenotypes in Alzheimer's Disease models. Neuron. 2018;97(5):1032–48. e5.
31. Karch CM, Goate AM. Alzheimer's disease risk genes and mechanisms of disease pathogenesis. Biol Psychiatry. 2015;77(1):43–51.
32. Efthymiou AG, Goate AM. Late onset Alzheimer's disease genetics implicates microglial pathways in disease risk. Mol Neurodegener. 2017;12(1):43.
33. Keren-Shaul H, Spinrad A, Weiner A, Matcovitch-Natan O, Dvir-Szternfeld R, Ulland TK, David E, Baruch K, Lara-Astaiso D, Toth B, Itzkovitz S, Colonna M, Schwartz M, Amit I. A unique microglia type associated with restricting development of Alzheimer's disease. Cell. 2017;169(7):1276-e129017.
34. Wang Y, Zhang X, Song Q, Hou Y, Liu J, Sun Y, Wang P. Characterization of the chromatin accessibility in an Alzheimer's disease (AD) mouse model. Alzheimers Res Ther. 2020;12(1):29.
35. Chen Y, Liu Z, Gong P, Zhang H, Chen Y, Yao S, Li W, Zhang Y, Yu Y. The chemerin/CMKLR1 axis is involved in the recruitment of microglia to abeta deposition through p38 MAPK pathway. Int J Mol Sci. 2022;23(16):9041.
36. Zhang Y, Xu N, Ding Y, Zhang Y, Li Q, Flores J, Haghighiabyaneh M, Doycheva D, Tang J, Zhang JH. Chemerin suppresses neuroinflammation and improves neurological recovery via CaMKK2/AMPK/Nrf2 pathway after germinal matrix hemorrhage in neonatal rats. Brain Behav Immun. 2018;70:179–93.
37. Halle A, Hornung V, Petzold GC, Stewart CR, Monks BG, Reinheckel T, Fitzgerald KA, Latz E, Moore KJ, Golenbock DT. The NALP3 inflammasome is involved in the innate immune response to amyloid-beta. Nat Immunol. 2008;9(8):857–65.
38. Ising C, Venegas C, Zhang S, Scheiblich H, Schmidt SV, Vieira-Saecker A, Schwartz S, Albasset S, McManus RM, Tejera D, Griep A, Santarelli F, Brosseron F, Opitz S, Stunden J, Merten M, Kayed R, Golenbock DT, Blum D, Latz E, Buee L, Heneka MT. NLRP3 inflammasome activation drives tau pathology. Nature. 2019;575(7784):669–73.
39. Liang Z, Han L, Sun D, Chen Y, Wu Q, Zhang L, Zhou M, Chen D. Chemerin-induced macrophages pyroptosis in fetal brain tissue leads to cognitive disorder in offspring of diabetic dams. J Neuroinflammation. 2019;16(1):226.
40. Xie Y, Huang Y, Ling X, Qin H, Wang M, Luo B. Chemerin/CMKLR1 Axis promotes inflammation and pyroptosis by activating NLRP3 inflammasome in diabetic cardiomyopathy rat. Front Physiol. 2020;11:381.

Publisher's note